LA-UR- 09-00072

Title:

Decamethylytterbocene Complexes of Bipyridines and Diazabutadienes: Multiconfigurational Ground States and Open-shell Singlet Formation

Author(s):

Corwin H. Booth, Marc D. Walter, Daniel Kazhdan, Yung-Jin Hu, Wayne W. Lukens, Eric D. Bauer, Laurent Maron, Odile Eisenstein, and Richard A. Andersen

Intended for:

J. American Chemical Society

Decamethylytterbocene Complexes of Bipyridines and Diazabutadienes: Multiconfigurational Ground States and Open-shell Singlet Formation

Corwin H. Booth,[*,†] *Marc D. Walter,*[†,‡] *Daniel Kazhdan,*[†,‡] *Yung-Jin Hu,*[†,‡] *Wayne W. Lukens,*[†] *Eric D. Bauer,*[§] *Laurent Maron,*[#] *Odile Eisenstein,*[|] *and Richard A. Andersen*[†,‡]

Contribution from the Chemical Sciences Division, Lawrence Berkeley National Laboratory, Berkeley, California 94720, Department of Chemistry, University of California, Berkeley, California 94720, Materials Physics and Applications Division, Los Alamos National Laboratory, Los Alamos, New Mexico 87545, LPCNO, CNRS-UPS-INSA, INSA Toulouse, 137 Avenue de Rangueil, 31077 Toulouse, France, Institut Charles Gerhardt Montpellier, UMR 5253 CNRS-UM2-ENSCM-UM1, Université Montpellier 2, cc1501, 34095 Montpellier cedex 05 France

AUTHOR EMAIL ADDRESS: chbooth@lbl.gov

*Corresponding author. E-mail: chbooth@lbl.gov, Phone: 510-486-6079, FAX: 510-486-5596

[†] Lawrence Berkeley National Laboratory.

[‡] University of California, Berkeley.

[§] Los Alamos National Laboratory.

[#] LPCNO, CNRS-UPS-INSA, INSA Toulouse.

[|] Université Montpellier 2.

Draft 12/8/2008. 8:40:26 AM

ABSTRACT. Partial ytterbium *f*-orbital occupancy (i.e. intermediate valence) and open-shell singlet formation are established for a variety of bipyridine and diazabutadiene adducts to decamethylytterbocene, $(C_5Me_5)_2Yb$ or $Cp^*{}_2Yb$. Data used to support this claim includes ytterbium valence measurements using Yb L_{III}-edge x-ray absorption near-edge structure (XANES) spectroscopy, magnetic susceptibility and Complete Active Space Self-Consistent Field (CASSCF) multiconfigurational calculations, as well as structural measurements compared to density-functional theory (DFT) calculations. The CASSCF calculations indicate that the intermediate valence is the result of a multiconfigurational ground state wave function that has both an open-shell singlet f^{13} and a closed-shell singlet f^{14} component. A number of other competing theories for the unusual magnetism in these materials are ruled out by the presence of intermediate valence and its lack of any significant temperature dependence. These results have implications for understanding chemical bonding not only in organolanthanide complexes, but also for organometallic chemistry in general, as well as understanding magnetic interactions in nanoparticles and devices.

1. Introduction

The canonical view of magnetism and bonding in lanthanide organometallic compounds is that of localized *f*-orbitals split by interactions with ligand orbitals, but not participating in bonding. This rule, of course, has some well known exceptions, particularly in solid-state intermetallics.[1-3] Two features of *f*-orbital bonding in these intermetallic systems are noteworthy. First, a reduced magnetic moment at low temperatures is typically observed, and second, a theoretical understanding cannot be obtained without including higher-order (many-body) interactions than are typically provided by a molecular theoretical method such as Density Functional Theory (DFT). Recently, several N-heterocyclic base adducts of ytterbocene of the form $Cp^*_2Yb(L)$, where Cp* = pentamethylcyclopentadienyl = C_5Me_5 and *L* is one of several bipy (bipy = 2,2′-bipyridine),[4-6] dad (dad = 1,4-diazabutadiene),[7] and related[6, 8] adducts, have been shown to display unusual magnetic properties involving an apparently reduced magnetic moment of the complex, corresponding to an extremely strong antiferromagnetic coupling constant. For instance, using the temperature of the peak in the magnetic susceptibility as an estimate of twice the coupling constant, $\Im$, the bipy and dad adducts have $\Im \approx -100\ \text{cm}^{-1}$, whereas $\Im$ between a lanthanide and a radical is typically smaller than $-10\ \text{cm}^{-1}$.[9-15] The origin of the reduced moment in these molecules has been controversial. The heart of the controversy has been whether the reduced moment is caused by some type of antiferromagnetic coupling (mostly intramolecular, as shown by correlating solid-state magnetism and solution NMR spectra[5, 7]), or is due to the electronic structure on the metal center or the molecule.

In this article, we explore the ubiquity of such behavior in this class of molecules and the nature of this unusual magnetic interaction with measurements of the magnetic susceptibility and the x-ray absorption near-edge structure (XANES). A systematic relationship is observed between the effective valence of the ytterbium atoms and the magnetism in these molecules, indicating that as the ytterbium valence moves from Yb(III), $4f^{13}$, toward Yb(II), $4f^{14}$, an open-shell singlet ground state develops that becomes more stable as the f^{14} contribution increases. The magnetism of these materials is thus related to the degree of intermediate valence. Here, the term "intermediate valence" denotes a fractional, or non-integer valence. For example, the valence of ytterbium in $Cp^*_2Yb(pyridine)_2$ is two, Yb(II), and the Yb atom has a closed shell $4f^{14}$ electron configuration, consistent with its physical properties. Similarly, the valence of ytterbium in [Cp*$_2$Yb(bipy)]+[I]- is unambiguously three, Yb(III), and the atom has an open shell $4f^{13}$ electron configuration, consistent with its physical properties. However, the valence of the ytterbium atom in $Cp^*_2Yb(bipy)$ is neither two nor three; rather, it is in between these extreme values, *i.e.*, it has an intermediate valence. The physical studies reported in this article give the value of the valence from which a physical model, supported by calculations, is developed to rationalize why the complex has intermediate valence.

The presence of intermediate valence in the ytterbium atoms, and the lack of a strong temperature dependence of this valence, rules out several other interpretations of the magnetism, such as those invoking valence tautomerism or crystal-field interactions. These data therefore point to the formation of a multiconfigurational, open-shell singlet ground-state with anomalously strong antiferromagnetic coupling between the moments on the metal and the aromatic ligand. Similar behavior was predicted for cerocene[16-18] ($Ce(cot)_2$, cot = cyclooctatetraene = C_8H_8) and supported by experiments on cerocene,[19] substituted cerocenes,[20, 21] the isoelectronic compounds Pn^*_2Ce (Pn* = permethylpentalene = C_8Me_6)[22] and $Ce[C_8H_4(Si^iPr_3\text{-}1,4)_2]_2$,[23] as well as $[Ce(\eta\text{-}C_5H_5)_3]^+$,[24] Cp^*_2Yb(terpy = 2,2′:6′,2″-terpyridine),[8] and $Cp^*_2Yb(bipy)$.[19] This interpretation is further supported by Multireference Configuration Interaction including Single and Double excitation (MRCISD) calculations (previously only available for cerocene) using the Complete Active Space Self-Consistent Field (CASSCF) method on $(C_5H_5)_2Yb(bipy)$ and $(C_5H_5)_2Yb$(dad(H)-tBu) molecules, which also highlight the structural implications of such intermediate valent Yb states. Therefore, these results emphasize the importance of a higher-order, multiconfigurational approach in determining the nature of the chemical bond in lanthanide organometallics in which an *f* electron on the metal centers can couple to delocalized π electrons on the ligand.

Below Yb L_{III}-edge XANES and magnetic susceptibility measurements are reported on several bipy and dad adducts to Cp*$_2$Yb of the type Cp*$_2$Yb(*L*) (Scheme 1), where *L* is bipy, and 4,4'-disubstituted bipyridines and 1,4-diazabutadiene derivatives, including purely di- and trivalent Yb complexes. These bipy and dad ligands were chosen over related 4,4′-alkyl substituted 2,2′-biyridines such as the 4,4′-dimethyl-2,2′-bipyridine or 4,4′-di(tert-butyl-2,2′-bipyridine),^{5} the former do not display any obvious phase transitions or other hysteretic behavior, and, as will be shown below, do not exhibit any obvious temperature dependence to the Yb valence. Examples of ytterbocene complexes that display strong temperature dependence of the Yb valence will be considered in a future paper.

Scheme 1. Schematic diagram showing bipyridyl and diazabutadiene adducts discussed in the present work.

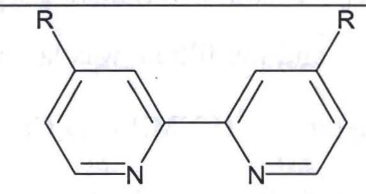

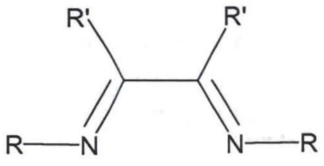

R	abbreviation	R	R'	abbreviation
H	bipy	H	C(Me)$_3$	dad(H)-*t*-Bu
OMe	bipy-OMe	H	CH(Me)$_2$	dad(H)-*i*-Pr
C$_6$H$_5$	bipy-phenyl	H	adamantyl	dad(H)-adamantyl
CO$_2$Me	bipy-CO$_2$Me	H	C$_6$H$_4$-p-tolyl	dad(H)-*p*-tolyl
CO$_2$Et	bipy-CO$_2$Et	Me	C$_6$H$_4$-OMe	dad(Me)-*p*-anisyl
		H	C$_6$H$_2$-2,4,6-Me$_3$	dad(H)-mesityl

2. Experimental Section

General synthesis. Samples were prepared as previously described,[4, 5, 7, 25] except as noted below.

Preparation of Cp*$_2$La(OTf)(pyridine). MgCp*$_2$ (6.11 g, 2.7 mmol) and dry La(OTf)$_3$ (12.15 g, 2.7 mmol) in 50 mL of a 1:10 pyridine:toluene were stirred overnight. The green-yellow solution was then taken to dryness and the green-yellow residue was dissolved in 300 mL of diethylether. The suspension was filtered, and the filtrate was concentrated to 100 mL, then warmed to re-dissolve the precipitate and the solution was cooled to -20 °C. Light green crystals of Cp*$_2$La(OTf)(pyridine) formed. Yield 2.40 g (18 %). ^{1}H NMR (C_6D_6): δ 1.92 (s, 30H), 6.56 (t, 1H, $J = 7$ Hz), 6.84 (t, 2H, $J = 8$ Hz), 8.32 (d, 2H, $J = 5$ Hz). ^{19}F NMR (C_6D_6): δ -76.7 (s). Anal. Calcd for $C_{26}H_{35}NF_3LaO_3S$: C, 48.98; H, 5.53; N, 2.20. Found C, 49.12; H, 5.26; N, 2.20. M.P.: 363-367 °C.

Preparation of Cp*$_2$La(2,2'-bipyridine)(OTf). Cp*$_2$La(OTf)(pyridine) (1.2g, 1.9 mmol) and bipy (0.29g, 1.9 mmol) were mixed in 50 mL of pentane with stirring. After stirring the suspension overnight, the solvent was filtered, the red powder was dissolved in 5 mL of CH_2Cl_2 and the filtrate was layered with pentane. Red crystals formed over the course of a week. Yield 0.48g (36%). ^{1}H NMR (CD_2Cl_2): δ 1.73 (s, 30H), 7.70 (t, 2H, $J = 6$ Hz), 8.14 (td, 2H, $J = 8$ Hz, $J = 2$ Hz), 8.26 (d, 2H, $J = 8$ Hz), 8.92 (2H, $\upsilon_{1/2} = 40$ Hz). ^{19}F NMR (CD_2Cl_2): δ -76.99 (s). Anal. Calcd for $C_{31}H_{38}N_2F_3LaO_3$: C, 52.10; H, 5.36; N, 3.92. Found C, 51.74; H, 5.00; N, 3.81.

Preparation of Cp*$_2$La(2,2'-bipyridine). Cp*$_2$La(2,2'-bipyridine)(OTf) (1.1 g, 1.6 mmol) was added to sodium amalgam formed by dissolving Na (0.04 g, 1.9 mmol) in Hg (38 g, 188 mmol). Toluene (100 mL) was added and the dark red solution was stirred overnight. The toluene suspension was filtered and the filtrate was taken to dryness. The dark red residue was dissolved in 60 mL of pentane, the suspension was filtered, and the filtrate was concentrated to 20 mL, heated to redissolve the Cp*$_2$La(2,2'-bipyridine) and then cooled to -20 °C. Dark red crystals were obtained. Yield 0.70 g (79%). ^{1}H NMR (C_6D_6): 3.39 ($\upsilon_{1/2} = 120$ Hz); the 2,2'-bipyridine resonances were not found. Anal. Calcd for $C_{30}H_{38}LaN_2$: C, 63.71; H, 6.77; N, 4.95. Found: C, 63.45; H, 6.97; N, 4.87. M.P. 310-312 °C. IR (Nujol mull): 2917 (vs), 2724 (w), 1539 (w), 1463 (s), 1417 (w), 1377 (s), 1276 (m), 1260 (m), 1205 (m), 1169 (w), 1146 (m), 1076 (m), 998 (m), 942 (s), 822 (w), 743 (w), 715 (s), 676 (m), 642 (m), 604 (w). UV-Vis (C_6H_{12}) (λ_{max}, ε x 10^{-3} $Lmol^{-1}cm^{-1}$): 930 (1.36), 812 (2.07), 368 (10.10).

Preparation of Cp*$_2$Yb(OTf)(pyridine). MgCp*$_2$ (6.1 g, 20.8 mmol) was stirred with dry Yb(OTf)$_3$ (12.9g, 20.8 mmol) in 50 mL of a 1:10 mixture of pyridine:toluene. The purple solution was warmed and stirred overnight. The solution was then taken to dryness and the purple residue was dissolved in 100 mL of diethylether. The suspension was filtered and the filtrate was concentrated to 50 mL, warmed to dissolve the Cp*$_2$Yb(OTf)(pyridine) and cooled to -20 °C overnight. Dark purple block crystals of Cp*$_2$Yb(OTf)(pyridine) formed. Yield 12.6g (90%). ^{1}H NMR (C_6D_6): δ 3.83 (30H, $\upsilon_{1/2}$ = 60 Hz), 25.54 (1H, $\upsilon_{1/2}$ = 80 Hz). The ortho and meta hydrogens were not observed at 20 °C. ^{19}F NMR (C_6D_6): δ -51.0 (s) Anal. Calcd for $C_{26}H_{35}NF_3O_3SYb$: C, 46.49; H, 5.25; N, 2.09. Found C, 46.35; H, 4.94; N, 2.43. M.P.: 211 °C.

Preparation of [Cp*$_2$Yb(N,N'-bis(p-tolyl)-1,4-diazadienyl)][BPh$_4$]. Cp*$_2$Yb(OTf)(pyridine) (0.65 g, 0.97 mmol), N,N'-bis-(p-tolyl)-1,4-diazadiene (0.24 g, 0.97 mmol) and NaBPh$_4$ (1.0 g, 2.8 mmol) were stirred in 50 mL of pentane overnight. The pentane was filtered, the brown residue was dissolved in 10 mL of CH_2Cl_2, filtered and the filtrate was layered with 50 mL of pentane. Brown plate-like crystals of [Cp*$_2$Yb(dad(H)-p-tolyl)][BPh$_4$] formed. Yield 0.36g (37%). ^{1}H NMR (CD_2Cl_2): δ -35.53 (2H, $\upsilon_{1/2}$ = 80 Hz), -3.21 (30H, $\upsilon_{1/2}$ = 200 Hz), -0.649 (4H, $\upsilon_{1/2}$ = 60 Hz), 1.19 (8H, $\upsilon_{1/2}$ = 40 Hz), 2.24 (8H, $\upsilon_{1/2}$ = 40 Hz), 24.54 (6H, $\upsilon_{1/2}$ = 4 Hz), 53.92 (2H, $\upsilon_{1/2}$ = 800 Hz). One resonance due to 4H's, perhaps those of the ortho-H's of the p-tolyl ring, was not observed at 20°C. ^{11}B NMR (CD_2Cl_2): δ -12.78 ($\upsilon_{1/2}$ = 8 Hz). Anal.Calcd for $C_{60}H_{66}N_2BYb$: C, 72.14; H, 6.66; N 2.80. Found C, 69.82; H, 6.26; N, 2.97. A crystal suitable for X-ray diffraction was selected; full crystallographic details are available as Supporting Information.

X-ray absorption near-edge structure (XANES) spectroscopy. The samples for x-ray absorption measurements were prepared by mixing 3-10 mg of sample with dried boron nitride in an inert atmosphere (Ar or N_2) glove box and loading the mixture into a slotted, multiple-sample aluminum holder with indium sealed aluminized mylar windows. These holders provide sufficient sample protection that the sample integrity was not compromised during transportation in a container backfilled with nitrogen or argon to the Stanford Synchrotron Radiation Laboratory (SSRL). X-ray absorption data were collected primarily on beam line 11-2 using an unfocused, uncollimated beam with energy resolution (< 0.7 eV) far narrower than the energy width of the edge due to the core-hole lifetime ($E_\tau \approx 4.2$ eV[26]). A spectrum of Yb_2O_3 was collected simultaneously as an energy reference, and the incident energy was calibrated by arbitrarily setting the first inflection point in the main edge of the Yb_2O_3 sample to 8943 eV. All sample holders were loaded into an evacuated liquid helium flow cryostat at the beamline and data were collected at temperatures between 30 and 300 K using a half-tuned Si(220) double crystal monochromator. Sample integrity was easily verified by observing the absorption spectra of an oxygen "canary" that is always loaded into one slot of each multislot sample holder, typically a divalent ytterbocene such as $Cp^*_2Yb(py)_2$ or $Cp^*_2Yb(OEt_2)$.

XANES data are widely used to extract the effective valence in Yb systems, and the technique is generally considered to be accurate within an absolute (systematic) error of about 5% (for instance, a good correspondence between the valence and magnetism in various Yb alloys has been observed[27]). The best way to extract the valence is to obtain model spectra for the di- and trivalent components. However, in the present case, the lutetium analogs, which could be used as models for either of these components, were not available. Instead the XANES spectra were fitted to a combination of pseudo-Voigt functions to extract the relative weight of the di- and trivalent Yb features. Each spectrum was fitted to in integrated pseudo-Voigt to simulate the main edge, together with a single pseudo-Voigt each for the divalent and trivalent resonances, and lastly, a pseudo-Voigt with negative amplitude to simulate the first extended x-ray absorption fine-structure (due to the local crystal structure[28]) . We have compared this method to using Lu L_{III} edge spectra on a number of intermetallic intermediate valent systems, notably the $Yb_{1-x}Lu_xAl_3$ series, and find the results are with in about 3-5% of each other, the absolute error typically ascribed to this technique.

Magnetometry. Magnetic measurements were conducted in a 7 T Quantum Design MPMS magnetometer utilizing a superconducting quantum interference device (SQUID). Between 10 and 25 mg of sample were sealed in evacuated quartz tubes while held in place with ~5 mg of quartz wool. This method provides a very small and reliable container correction, typically of about -2×10^{-5} emu. The data are also corrected for the overall diamagnetism of the molecule using Pascal constants.[29] The accuracy of these methods has been verified in measurements of ferrocene, giving the expected zero moment within 5×10^{-6} emu/mol.[25] Data were collected at two fields (5 kOe or 40 kOe) depending on what data are available over a given temperature range. Low-field data were best for subtracting out impurity contributions, and they were fully consistent with the high-field data obtained at high temperatures. Impurity contributions (i.e. "Curie tails") for $Cp^*_2Yb(py)_2$ and the dad adducts were estimated by fitting the low temperature data to a constant, χ_0, plus a Curie-Weiss term $C_{\mathrm{imp}}/(T-\Theta_W)$ and taking the impurity fraction as $C_{\mathrm{imp}}/C_{J=7/2}$. This procedure produced poor quality fits for the bipy adducts, and therefore the $Cp^*_2Yb(py)_2$ data were used as a model of the impurity contribution.

Electron paramagnetic resonance (EPR) spectroscopy. EPR spectra were obtained at room temperature with a Varian E-12 spectrometer equipped with an EIP-547 microwave frequency counter and a Varian E-500 gaussmeter, and were calibrated using 2,2-diphenyl-1-picrylhydrazyl (DPPH, g = 2.0036).

Computational details. The ytterbium center was treated with either a small core relativistic pseudopotential (RECP) (explicit 4*f* shell)[30] in combination with its adapted basis set or a *f*-in-core (large core) pseudopotential from the Stuttgart group[31, 32] with the optimized basis set augmented by a set of polarization functions (namely *f* functions). The carbon, nitrogen, oxygen and hydrogen atoms were treated with an all-electron double-ζ, 6-31G(*d,p*), basis set.[33] All the calculations were carried out with the Gaussian 98 suite of programs[34] either at the DFT level using the B3PW91[35, 36] hybrid functional or at the CASSCF level. The geometry optimizations were performed without any symmetry constraints either at the DFT or the CASSCF levels. A vibrational analysis was done using analytic determination of the frequencies in a harmonic approximation. The UV spectra were simulated by using the time-dependent DFT approach.[37]

Table 1. Summary of available data and fit results on $Cp^*_2Yb(L)$ compounds.

Compound	**Yb(III) imp.**[a] **(%)**	χ_0[a] **(emu/mol)**	**T(χ_{max})**[b] **(K)**	n_f[c]	**C2-C2′**	**Ligand Redox potential**[d]
$[Cp^*_2Yb(bipy)]^+\ I^-$				1.01(2)	1.492(4)[j]	-2.60
$Cp^*_2Yb(bipy\text{-}phenyl)$	4.2	0.0031	390	0.89(2)		-2.34
$Cp^*_2Yb(bipy\text{-}CO_2Me)$	2.6	0.0025	355	0.84(2)		-2.03
$Cp^*_2Yb(bipy)$	0.5	0.00176	380	0.83(2)	1.426(5)	-2.60
$Cp_2Yb(bipy)$	0.8	0.00024		0.30(1)		-2.60
$Cp^*_2Yb(bipy\text{-}OMe)$	0.6	0.00042		0.13(9)		-2.88
$Cp^*_2Yb(py)_2$	0.5	-0.00001		0.2(1)		
$Cp^*_2Yb(Et_2O)$	1.6	0.00007		0.07(1)		
$[Cp^*_2Yb(dad(H)\text{-}p\text{-}tolyl)]^+\ [BPh_4]^-$				0.95(2)	1.478(9)	-1.88
$Cp^*_2Yb(dad(H)\text{-}mesityl)$	3.1	0.0065	140	0.93(1)	1.413(15)	-1.91[g]
$Cp^*_2Yb(dad(H)\text{-}p\text{-}tolyl)$	5.4	0.0044	260	0.94(1)	1.380(9)	-1.88
$Cp^*_2Yb(dad(Me)\text{-}p\text{-}anisyl)$	6.1	0.0038	260	0.94(1)		-2.33
$Cp^*_2Yb(dad(H)\text{-}i\text{-}Pr)$ #1	5.6	0.0035	-	0.91(1)		-2.44[h]
$Cp^*_2Yb(dad(H)\text{-}i\text{-}Pr)$ #2[f]	10.5	0.0028	360	0.89(1)		
$Cp^*_2Yb(dad(H)\text{-}adamantyl)$	0.05	0.0031	330	0.91(1)	1.397(4)[e]	-2.61[i]
$Cp^*_2Yb(dad(H)\text{-}t\text{-}Bu)$	0.04	0.0025	360	0.89(1)	1.398(5)	-2.61

[a] Yb(III) impurity and χ_0 are determined by fitting $\chi(T)$ from **Figure 4** at low temperature with a constant (χ_0) plus the magnetic susceptibility of either $[Cp^*_2Yb(bipy)]^+[I]^-$ as an appropriate trivalent ytterbium reference for the bipy materials, or a Curie-Weiss function for the dad materials.

[b] The temperature where $\chi(T)$ goes through a maximum value χ_{max}.

[c] The number of f-holes, that is, the valence $v=2+n_f$. Errors are from the covariance matrix in the fit, consistent with random errors between scans. Absolute errors are between 3-5%, see text.

[d] Ligand redox potentials are as reported by Ref. [7], unless otherwise noted.

[e] Ref. [38]

[f] These parameters were obtained on an *i*-Pr sample with higher impurity content; however, these impurities should have only a small effect on these values, especially for $T(\chi_{max})$.

[g] Derived by inference from the 2,6-methyl substituted derivative (mes= 2,4,6-methyl substituted derivative).[39, 40]

[h] Derived from the cyclohexyl derivative.[39, 40]

[i] Derived by inference from the reduction potential of dad(H)-*t*-Bu).

[j] This value is derived from the C2-C2′ bond distance in $[(Me_5C_5)_2Yb(bipy)]^+[(Me_5C_5)2YbCl_2]^-$.[4]

3. Results: Experimental

XANES. XANES data at 20 K are displayed in **Figure 1**, and those of some selected bipy adducts at various temperatures in **Figure 2**. Data for $Cp^*_2Yb(py)_2$ are not shown, but agree well with the divalent Yb signal from $Cp^*_2Yb(OEt_2)$. The bipy adduct data in **Figure 1**a show the full range of expected behavior, starting from the nominally divalent $Cp^*_2Yb(OEt_2)$ spectra, then the intermediate valent $Cp^*_2Yb(bipy\text{-}CO_2Me)$ and $Cp^*_2Yb(bipy)$ spectra, and finally the trivalent $[Cp_2^*Yb(bipy)]^+I^-$ spectra. The dad adduct data in **Figure 1**b are similar, although all are very close to trivalent with only a small (< 12% in all cases) divalent contribution. In spite of this nearly trivalent character, the subtle trends in the white line intensity and the shoulder at ~ 8939 eV between the dad adducts track the differences between these samples in their magnetic susceptibility traces (see below).

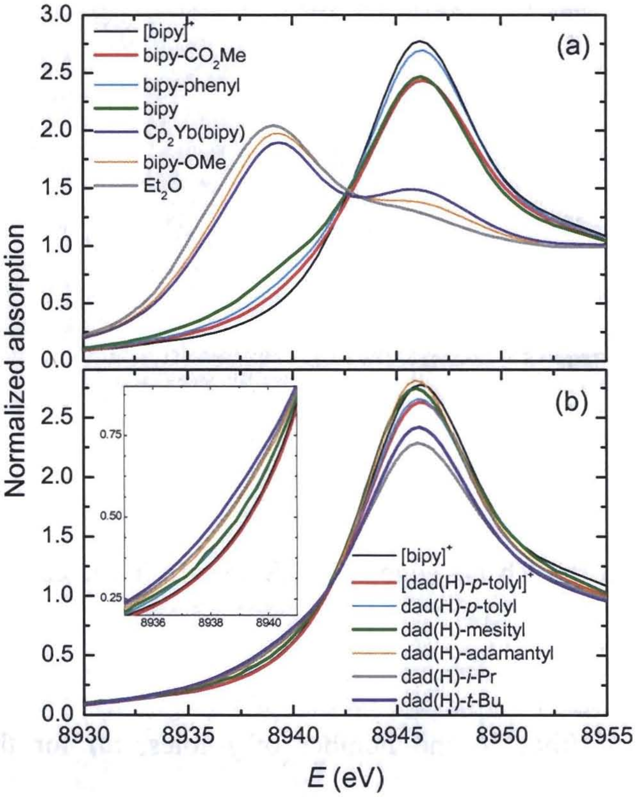

Figure 1. Yb L_{III}-edge XANES spectra at 20 K for most of the compounds discussed in the text. Panel (a) focuses on the bipy compounds, while panel (b) focuses on selected dad compounds. The inset of panel (b) is a magnification of the divalent shoulder of the dad data. All compounds are coordinated to Cp*, except as indicated.

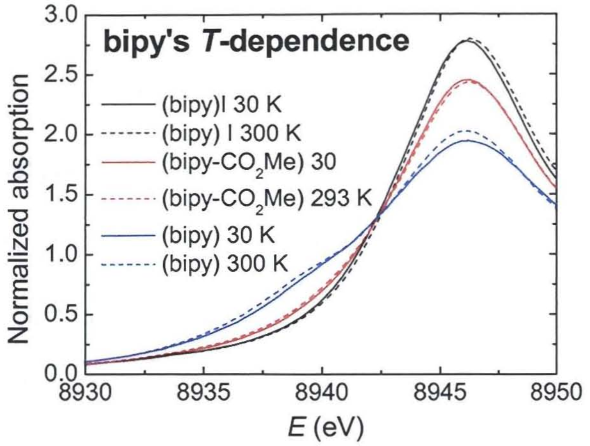

Figure 2. Yb L_{III}-edge XANES spectra at various temperatures as an example of any potential temperature dependence of the Yb valence in these materials. This level of reproducibility is similar to that obtained by collecting at a fixed temperature and looking at different parts of the same sample.

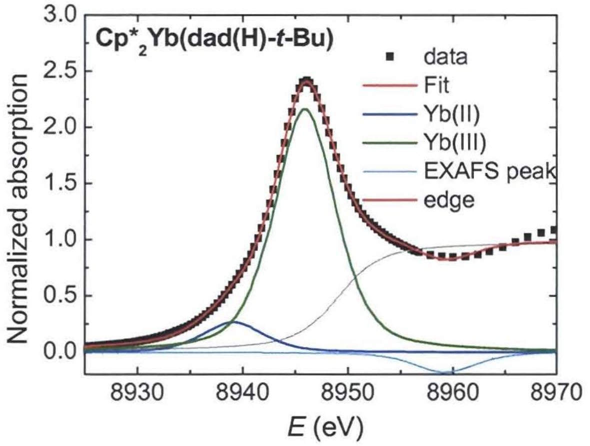

Figure 3. Example of use of pseudo-Voigt peaks to fit the Yb L_{III}-edge XANES spectra in the case of data from Cp*$_2$Yb(dad(H)-*t*-Bu).

An example of a fit for determining the valence (that is, the number of *f*-holes, n_f) for the Cp*$_2$Yb(dad(H)-tBu) data is shown in **Figure 3**. The valence data for all measured samples are summarized in Table 1. The Cp*$_2$Yb(bipy) complex has, for example, 83% trivalent character, while the dad complexes have between about 89 and 95% trivalent character. All of these data are collected at temperatures ranging from 20-300 K, and in some cases up to 450 K, and no measurable temperature dependence has been observed within 5% (*eg*. see **Figure 2**).

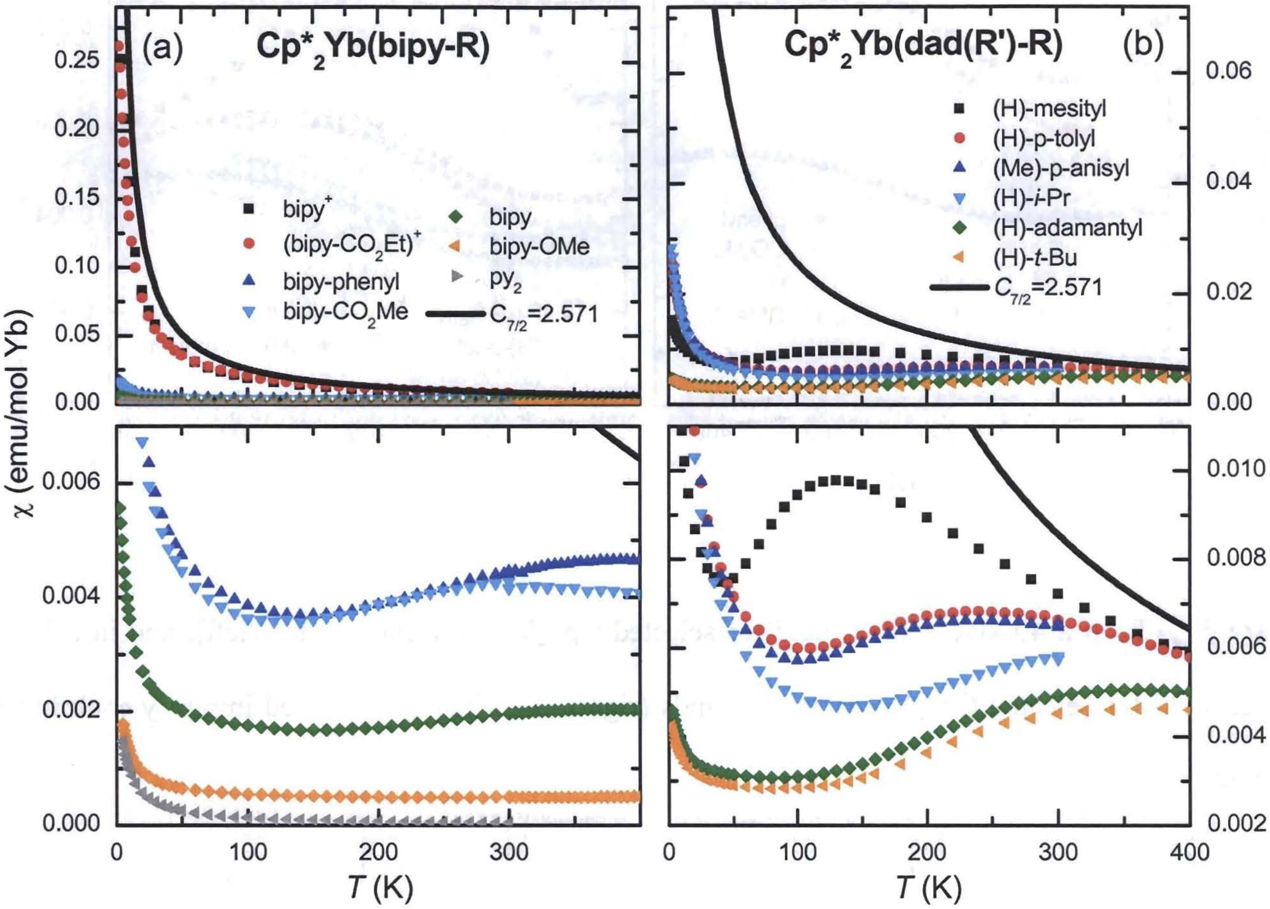

Figure 4. Magnetic susceptibility $\chi(T)$ in a 40 kOe applied field for the Cp*$_2$Yb bipy compounds (left panel) and Cp*$_2$Yb dad compounds (right panel), corrected for background and the diamagnetic contribution of the matrix. In addition to the compounds in Scheme 1, bipy$^+$=[Cp*$_2$Yb(bipy)]$^+$[I]$^-$ and (bipy-CO$_2$Et)$^+$ = Cp*$_2$Yb(bipy-CO$_2$Et)]$^+$[Cp*$_2$YbI$_2$]$^-$. Lower panels are magnifications of the upper panels. Data from Cp*$_2$Yb(OEt$_2$) and Cp*$_2$Yb(dad(H)-i-Pr) #2 are not shown for clarity. Some of these data have been published previously,[4, 5, 7] although not reported as $\chi(T)$.

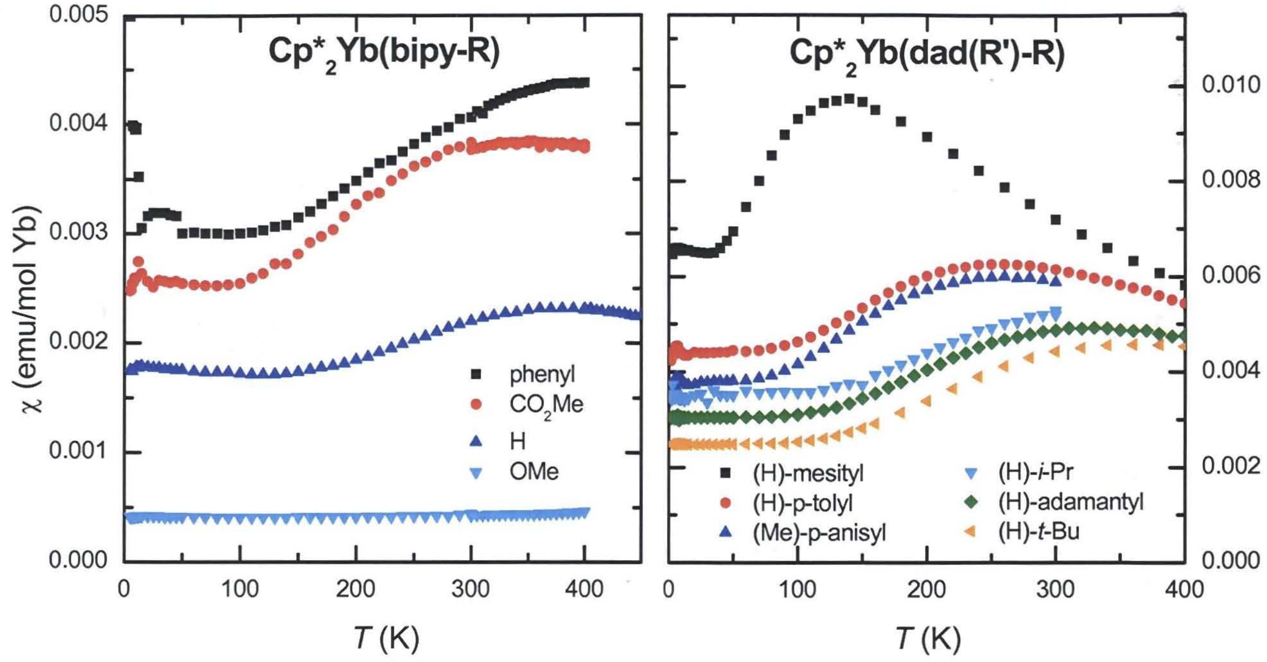

Figure 5. χ(T) in a 40 kOe applied field for selected Cp*$_2$Yb bipy compounds (left), and in a 5 kOe applied field for selected Cp*$_2$Yb dad compounds (right), all with the estimated impurity contribution removed.

Magnetic susceptibility and EPR results. The magnetic susceptibility, χ(*T*), for the bipy and dad adducts are displayed in **Figure 4** together with that expected for a free ion with $J = 7/2$: $\chi(T) = C_J/T$ with Curie constant $C_{7/2} = 2.571$. Each of these data fall into three general classes: (i) those exhibiting close to full trivalent, $J = 7/2$ magnetism, *eg*. [Cp*$_2$Yb(bipy)]$^+$[I]$^-$, (ii) those that are nearly diamagnetic, *eg*. Cp*$_2$Yb(bipy-OMe) and (iii) those that are in between these two extremes and exhibit a local maximum in the susceptibility at temperatures > 100 K, *eg*. Cp*$_2$Yb(bipy-CO$_2$Me). Those data with small magnetic moments at low temperature, namely, those in classes (ii) and (iii), also show a sharp upturn in χ(*T*) with decreasing *T*. We ascribe this upturn to impurities, as evidenced by its saturation [?] in applied field, indicative of a small amount of a high-moment impurity, and by its irreproducibility in different independently prepared samples of the same compound.[4, 5, 41] For instance, we have measured several samples of $Cp^*_2Yb(bipy)$ over more than 25 years in different sample containment schemes and the behavior above about 100 K is always very similar, regardless of the magnitude of the so-called impurity-induced "Curie tails." (Figure S1). The magnitude of these Curie tails corresponds to $< 5\%$ (usually less) of a Yb(III) impurity, potentially caused by small amounts of hydrolysis or oxidation. The contributions from these Curie-tails may be subtracted to obtain the underlying susceptibilities of the $Cp^*_2Yb(L)$ complexes as shown in

Figure 5.[19] These subtracted data show that many samples exhibit temperature-independent paramagnetism (TIP) at the lowest temperatures. The results, such as the magnitude of TIP (χ_0), are summarized in Table 1.

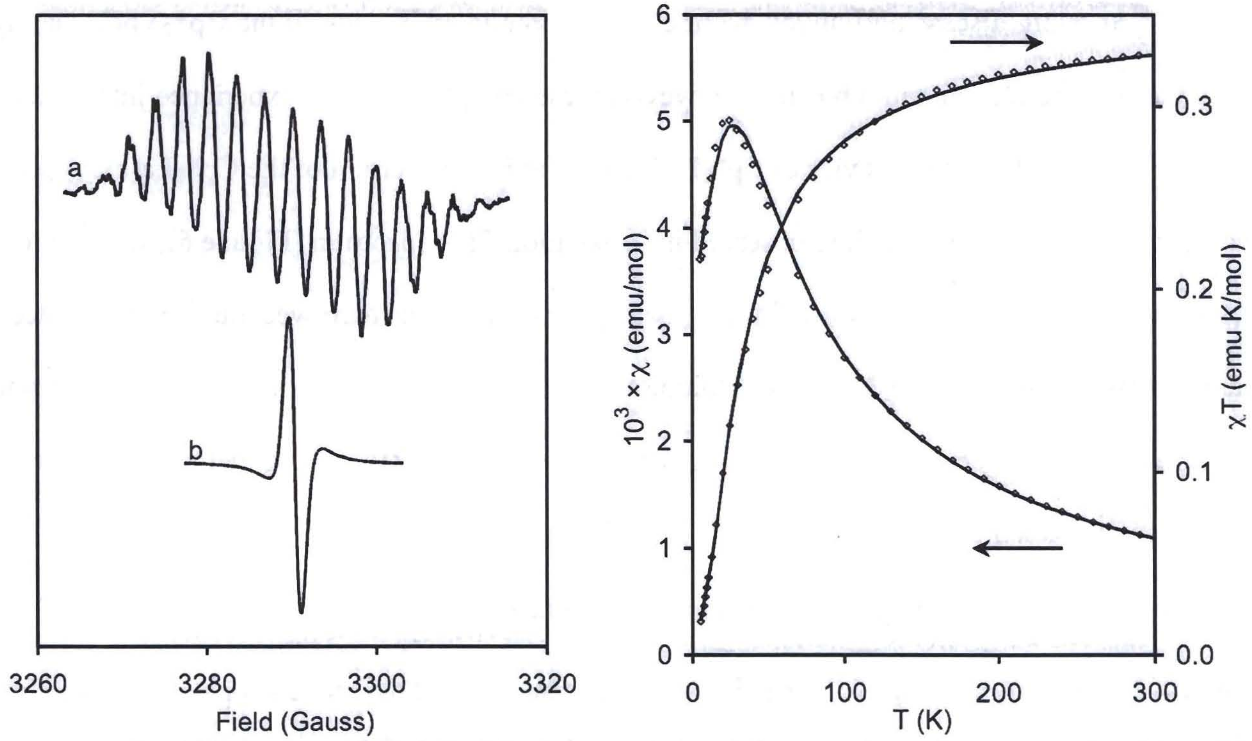

Figure 6. Left: EPR spectra of $Cp^*_2La(bipy)$ in methylcyclohexane (a) and as a powder (b) at 294 K. Right: Magnetic susceptibility of $Cp^*_2La(bipy)$. Data are shown as dots; the fit to eq 2 is shown as lines.

As shown by the XANES results, the complexes in class (ii) are largely $Cp^*_2Yb(II)(L)$ complexes with neutral diamine ligands with a small amount of $Cp^*_2Yb(III)^+(L)^-$ character while the complexes in class (iii) are largely $Cp^*_2Yb(III)^+(L)^-$ with a small amount of $Cp^*_2Yb(II)(L)$ character. Therefore, a plausible explanation for the reduced magnetic moment of the class (iii) complexes is antiferromagnetic coupling between the Yb(III) center and the ligand-based organic radical, which gives rise to an open-shell singlet ground state. One difference between the susceptibility of the open-shell singlet and the closed-shell singlet is that a closed-shell singlet is diamagnetic in which any temperature-independent paramagnetism is due to interaction with relatively high-energy excited states while the open-shell singlet is a temperature-independent paramagnet. Although the total angular momentum of the open-shell singlet is zero, the orbital angular momentum of the open-shell singlet is not zero if the angular momenta of the coupled magnetic centers are not identical; that is, if their g-values are different.[42] The considerable TIP of the $Cp^*_2Yb(L)$ complexes depends on the difference between the g-value of the organic radical and that of the Yb-center as well as the magnitude of the coupling between them.[42]

The preceding discussion implies that the only magnetic interaction in the $Cp^*_2Yb(L)$ family is between the organic radical and Yb center; however, these complexes likely experience intermolecular coupling as illustrated by the behavior of Cp^*_2La(bipy). The EPR spectrum of the Cp^*_2La(bipy) powder shows none of the hyperfine coupling observed in its solution EPR spectrum (**Figure 6**), which strongly suggests that the EPR spectrum of solid Cp^*_2La(bipy) is exchange narrowed due to intermolecular exchange between adjacent Cp^*_2La(bipy) complexes. This postulate is confirmed by the magnetic susceptibility of Cp^*_2La(bipy) shown in **Figure 6**, which clearly shows a reduced susceptibility indicative of antiferromagnetic coupling. The Hamiltonian for isotropic intermolecular exchange, as expected for the coupling of organic radicals in one-dimensional chains is $\mathcal{H}_{\mathcal{L}\cdot\mathcal{L}}=-\Im_{LL}(S_{L,\mathrm{i}}\bullet S_{L,\mathrm{i+1}}+S_{L,\mathrm{i}}\bullet S_{L,\mathrm{i-1}})$ or $\mathcal{H}_{\mathcal{L}\cdot\mathcal{L}}=-2\Im_{LL}(S_{L,\mathrm{i}}\bullet S_{L,\mathrm{i+1}})$, where $S_{L,\mathrm{i}}$ is adjacent to $S_{L,\mathrm{i+1}}$ and $S_{L,\mathrm{i-1}}$. Two models for the susceptibility of such systems are the infinite Heisenberg 1-dimensional chain model[43] and the Bonner-Fisher (BF) model,[44] the latter of which provides an accurate fit to the susceptibility of Cp^*_2La(bipy) as shown in **Figure 6**. The closed-form solution to the BF model, eq 2, is given by Estes et al.[45] where $x=|\Im|/k_BT$, and g=2.000 (from EPR), and all of the other symbols have their usual meanings; eq 2 is scaled by 0.95 to obtain the best fit to the data, presumably due to slight weighing errors and/or small amounts of impurity. Attempted correction of $\chi_{\mathcal{L}\cdot\mathcal{L}}$ for inter-chain interactions using the Molecular Field approach did not improve the fit to the data.[45]

$$\chi_{\mathrm{L\cdot L}} = \frac{\mathrm{N}g^2\mu_{\mathrm{B}}^2}{\mathrm{kT}}\left(\frac{0.25+0.14996\mathrm{x}+0.30094\mathrm{x}^2}{1+1.9862\mathrm{x}+0.6885\mathrm{x}^2+6.0626\mathrm{x}^3}\right) \qquad (2)$$

Because of the presence of intermolecular coupling, the model for the susceptibility of the ytterbocene complexes is more complicated than intramolecular coupling only between the organic radical and the Yb center, which is one of the reasons that no attempt was made to fit the susceptibility data for the Cp*$_2$Yb(*L*) complexes. The other reason is that the conventional approaches to fitting intramolecular coupling, Heisenberg or Ising models, fail for magnetic ions, such as the lanthanides, that have unquenched orbital angular momentum.[46] In addition to unquenched orbital angular momentum, the lanthanides often have low-lying excited states that contribute to the susceptibility over the temperature range examined here, which further complicates modeling the susceptibility. An elegant approach to this problem is outlined by Lines; however, it relies on a detailed understanding of the crystal field of the magnetic ions.[46] Attempts to extend this approach to lanthanides are not successful in describing the magnetism of coupled lanthanide ions due primarily to a mismatch between the theoretical description of the crystal field of a complex and its actual crystal field.[47] Despite the fact that the susceptibility cannot be successfully modeled at present, the strongest interaction in the Cp*$_2$Yb(*L*) complexes is clearly that between the organic radical and the Yb center as illustrated by the Curie-Weiss [?] temperatures of the susceptibilities of Cp*$_2$La(bipy) (25 K) and Cp*$_2$Yb(bipy) (380 K). Although the intermolecular coupling is important for understanding the details of the magnetic behavior in the Cp*$_2$Yb(*L*) systems, the much stronger interaction between the Yb center and the radical anion can be addressed without considering the intermolecular coupling.

4. Results: Computational

Multiconfigurational calculations were carried out using the CASSCF method, focusing on the Cp$_2$Yb(bipy) complex, where Cp=C$_5$H$_5$. These results should also be qualitatively applicable to the Cp* derivatives used in the experimental studies. Since the 4*f* shell and the LUMO π* level of the bipy ligand, hereafter referred to as π*, are close in energy, the geometry has been optimized at the CASSCF level by distributing 14 electrons into 8 orbitals, namely the 7 *f* and the π* orbitals. This configuration will lead to either to a singlet or a triplet ground state, reducing the problem to that of two particles (or two holes). The various electronic configurations that can be generated in a Generalized Valence Bond model are shown in Chart 1.

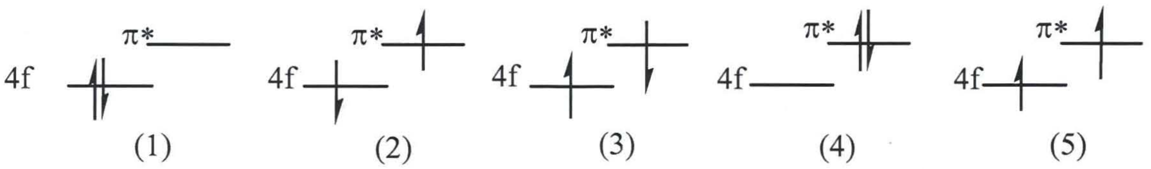

Chart 1. Valence bond model configurations. 4*f* spins are on particles starting with a f^{12} configuration. For example, configuration (1) is f^{14}. The first four configurations are magnetic singlets, and the last can only be described as a triplet.

In principle, the singlet state of the $Cp_2Yb(bipy)$ complex can be described by a mixing of the f^{14} configuration (1), f^{13} configurations (2 and 3) and the f^{12} configuration (4). The triplet is mainly defined by the f^{13} configuration (5). Thus, the geometry was optimized separately at the CASSCF level for the triplet state and for the open-shell singlet state. Interestingly, both geometry optimizations lead to the same structure, because the triplet and the open-shell singlet only differ by a spin flip of a single electron. The calculated structure is in good agreement with the experimental structure of $Cp^*_2Yb(bipy)$ (Table 2). The lowest singlet ground state[48] in the optimized wave function mainly consists of a mixing of configurations (1) and (2-3), namely, the f^{14} and f^{13} configurations of Yb. Moreover, configurations (2-3) provide the major contribution to the singlet state (89% after renormalization) whereas configuration (1) only contributes 11% to this state. Thus, the singlet state obtained is mainly open-shell with a dominant contribution of the valence electronic configuration $f^{13}\pi^*$, identical to the one of the triplet state, explaining the similarity between the optimized structures calculated for these two states. These results compare qualitatively well with the existence of intermediate valence in $Cp_2Yb(bipy)$ (n_f=0.30) and even better to the result of n_f=0.80 for $Cp^*_2Yb(bipy)$, reported in Table 1, although the presence of the methyl substituents on the Cp rings clearly have an influence. These substituent effects will be explored in a future publication.

The closed-shell singlet that is only due to configuration (1) in Chart 1 is optimized, also at the CASSCF level, and found to be 2.5 eV higher in energy than the open-shell singlet and triplet states. Thus, the closed-shell singlet state is not the ground state of the complex, but rather an excited state. In addition, the associated optimized geometry (Table 2) for the open-shell configurations compares well with the experimental data on $Cp^*_2Yb(bipy)$ [crystal structure data on $Cp_2Yb(bipy)$ is unavailable], in contrast with the calculation for the closed-shell configuration. Moreover, the open-shell system is calculated to be isoenergetic with the triplet state; the states differ by only 1 meV. Since more electronic configurations than were possible to include in the calculation will further lower the energy of the open-shell singlet relative to the triplet, these calculations indicate that the ground state of this system is indeed an open-shell singlet. These results therefore agree well with the experimental deductions outlined above.

Analyzing the geometrical parameters, the distance C2-C2′ in the bipy ligand and the C-C in the dad backbone, hereafter generically referred to as the C-C backbone distance, is strongly correlated with the Yb electronic configuration. This structural change is rationalized by the fact that the LUMO of the bipy ligand has bonding character between the C-C backbone carbons, and therefore populating the π^* shortens the C-C backbone distance, as previously outlined.[4] Since the CASSCF calculations are time-consuming calculations, faster calculations were carried out to further explore this structural aspect by freezing the f configuration on the ytterbium and including the f orbitals in the core. This method allows the geometry to be optimized for either a pure f^{13} or a pure f^{14} configuration. In the f^{13} configuration, the calculation has been carried out on a doublet spin state because the f^{13} configuration leads to an extra electron transferred to the lowest available π^* molecular orbital. The optimized geometries are identical with that obtained at the CASSCF level. In particular, the large core calculations reproduce the shortening of the C-C backbone distance from the closed-shell singlet to the open-shell singlet. This agreement originates from the fact that the open-shell ground state is mainly (89%) formed by an f^{13}

configuration. We therefore optimize the geometry for the two limit configurations (namely pure f^{13} or pure f^{14} configurations) using the *f*-in-core RECPs (see Experimental Section for computational details) and compare with the experiment when available, focusing on the C-C backbone distance as an indicator of the value of the ytterium valence.

Table 2. Comparison Between Selected Calculated and Experimentally Determined Bond Distances [Angstroms]

	Calculated		Experimental (X-ray diffraction)	
	$(C_5H_5)_2Yb(bipy)$ (f^{13})	$(C_5H_5)_2Yb(bipy)$ (f^{14})	$Cp^*_2Yb(bipy)$[a]	$Cp^*_2Yb(py)_2$[b]
Yb-C(ring) (mean)	2.66	2.80	2.62	2.74
Yb-C(ring) (range)	2.649-2.661	2.781-2.820	2.592(3)-2.614(3)	2.692(2)-2.769(7)
Yb-N (mean)	2.341	2.644	2.32	2.57
C2-C2′	1.430	1.489	1.435(9)	n/a

[a] Ref. [4] [b] Ref. [41]

	Calculated		Experimental (X-ray diffraction)	
	$(C_5H_5)_2Yb$(dad(H)-tBu) (f^{13})	$(C_5H_5)_2Yb$(dad(H)-tBu) (f^{14})	$(C_5H_5)_2Yb$(dad(H)-tBu)[a]	Cp^*_2Yb(dad(H)-tBu)[b]
Yb-C(ring) (mean)	2.68	2.81	2.60	2.69
Yb-C(ring) (range)	2.663-2.693	2.794-2.831	2.59(3)-2.60(3)	2.682(3)-2.716(4)
Yb-N (mean)	2.365	2.694	2.31	2.39
C2-C2′	1.403	1.474	1.398(10)	1.435

[a] Ref. [49] [b] Ref. [50]

Table 3. Calculated C-C Bond Distances

Complex	C2-C2′ (bipy) or C-C backbone (dad)	
	f^{13}	f^{14}
$(C_5H_5)_2Yb$(bipy-H)	1.430	1.489
$(C_5H_5)_2Yb$(bipy-CO_2Me)	1.446	1.489
$(C_5H_5)_2Yb$(bipy-OMe)	1.426	1.491
$(C_5H_5)_2Yb$(bipy-phenyl)	1.438	1.491

$(C_5H_5)_2Yb$(dad(H)-tBu)	1.403	1.473

This simplified methodology is applied to calculate the dad(H)-tBu and on 4,4′-substituted bipy (bipy-R) adducts, where R= H, OMe, CO_2Me and phenyl (see Tables 2 and 3) structures. In general, the Yb(II) and Yb(III) bipy models give a C2-C2′ distance of about 1.49 Å and 1.43 Å, respectively. The analogous distances are about 1.47 and 1.40 Å for the dad(H)-t-Bu adduct. For any substituent R in the 4,4′-position of the bipy adducts, the C2-C2′ distance is thus shorter for Yb(III) than for Yb(II). The small influence of R on C2-C2′ shows that the shape of π^*, and not only its energy, is influenced by the substituents. If the coefficients at the C2 and C2′ positions decrease in the π^* orbital, as in the case of CO_2Me, the effect of occupying the π^* orbital is less important. As can be seen in Table 1, these distances are consistent with known distances across the series, with most molecules having distances close to that expected from the Yb(III) model calculation, consistent with the XANES results that indicate the Yb in these molecules is close to trivalent. The exceptions are the longer C-C backbone distances in the $[Cp^*_2Yb(bipy)]^+I^-$ and $[Cp^*_2Yb(dad(H)\text{-}p\text{-tolyl})]^+[BPh_4]^-$ cation-anion pairs, as expected, since the anionic charge resides on the anion and not in the π^* orbital of the diazabutadiene and bipyridine ligands. While these calculations show that a short C-C backbone distance is an indication of a dominating Yb(III) configuration, the C-C backbone distance is influenced by the shape of the LUMO, as observed in the CO_2Me case. This distance, therefore, can only serve as a qualitative determination of the participation of the f^{13}-π^* configuration in the ground state.

The UV/Vis spectra for the same free bipy ligands (without coordination to the metal fragment) have also been calculated. The main result is that the π^* feature in L = bipy-OMe (λ_{max} = 280 nm) is at higher energy than that for bipy-CO_2Me (λ_{max} = 310 nm), bipy-phenyl (λ_{max} = 297 nm) or for bipy (λ_{max}= 293 nm). This transition energy is the HOMO-LUMO gap in the free ligand. However, there is a good correlation between the calculated absorption energy and the experimental reduction potential of the free ligand (**Figure 7**) which shows how the LUMO energy changes with substituents: a π-acceptor substituent (such as R= CO_2Me) lowers the LUMO, while a π-donor substituent, such as R= OMe, raises it. Thus, Yb is closer to divalent in L = bipy-OMe, while the others are closer to trivalent, in agreement with experiment. Accordingly the electron transfer from Yb(II) to the LUMO π^* of the ligand requires more energy for the bipy-OMe ligand than for the bipy-CO_2Me, bipy-phenyl, and bipy ligands. The reduction potentials and the absorption energies are therefore a qualitative indicator of the variation of the dominant configuration and the C-C backbone distance is a qualitative indicator of the relative $f^{14}/f^{13}\pi^*$ populations. A caveat is, however, that the C-C backbone distance behaves in a similar manner in the triplet and open-shell singlet configurations.

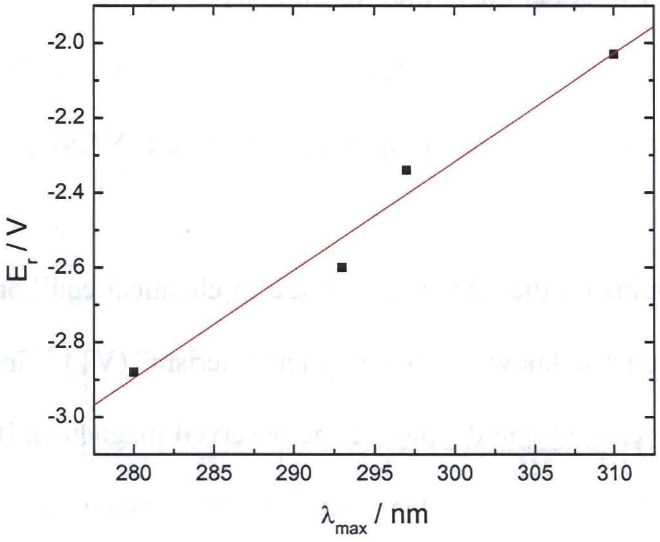

Figure 7. Correlation between experimentally determined reduction potential and calculated UV-vis absorption for the free bipy-R ligands.

5. Discussion

The experimental data and calculations reported above documents a very strong case for the presence of a multiconfigurational ground state, i.e. intermediate valence, forming an open-shell magnetic singlet in several adducts of $Cp^*_2Yb(L)$. Before discussing the wider implications of these results, particularly in light of similar experimental and theoretical results on cerocene, we consider two potential models for the magnetic behavior that these data rule out, namely, that the observed low magnetic moments are due either to differential populations of crystal field (CF) states, or to a chemical equilibrium between two valence states, such as occurs in valence tautomers. The essential difference between these models is the lack of temperature dependence of the ytterbium valence with temperature, as discussed below.

First, consider the possibility that the presence of a maximum in the susceptibility is primarily due to low-lying CF-split states. The ${}^2F_{7/2}$ free Yb(III) ion has a $J = 7/2$ ground state. In a low-symmetry CF, this state will split into linear combinations of $J = 7/2$, $5/2$, $3/2$ and $1/2$ states (in a cubic field, four doublets ensue[51]). In order to reproduce the magnetic susceptibility data, the ground or low energy ($T < 30$ K) state would have $C_J \sim 0.1$ emu·K/mol, and the energy to complete the full $J = 7/2$ multiplet would be $\Delta E_{\mathrm{cf}} \sim 40$ meV. This value of ΔE_{cf} is much larger than the splitting observed for other Yb compounds, where the full multiplet is typically recovered above 30 K (3 meV).[52] More importantly, Yb remains trivalent at all temperatures in a CF model, in clear disagreement with the XANES data, therefore ruling out this model.

A second possible model is that the $J = 7/2$ spins on the Yb(III) center are in chemical equilibrium with a diamagnetic Yb(II) center, that is, a situation also known as "valence tautomerism" (VT).[53] In this model, conventional, free-ion-type Curie-Weiss behavior could generate the observed magnetism if the Yb valence was not constant with temperature. The VT is due to thermally-induced charge transfer and has been widely observed, for instance, in Co/dioxolene complexes, such as the semiquinones. In Co-semiquinone, for instance, Co *K*-edge XANES data show the Co valence changes explain the bulk of the temperature dependence of the magnetism,[54] although many-body effects may be required for a complete understanding.[55] VT was originally listed as one possibility to account for the unusual magnetic behavior of $\mathrm{Cp^*_2Yb(bipy)}$,[4, 56] and had also been advocated,[6] and subsequently ruled out,[57] in $\mathrm{Cp^*_2Yb(terpy)}$. In order for VT to account for the magnetic susceptibility, the Yb(III) states must contribute the susceptibility expected for the full J=7/2 multiplet, while the remaining divalent Yb fraction has a fully occupied *f* shell, and is therefore diamagnetic. For the $\mathrm{Cp^*_2Yb(bipy)}$ complex, the f^{13} population would be about 30% at 300 K,[6] and should decrease at low temperature; both of these predictions are in disagreement with the Yb XANES data in **Figure 1** and **Figure 2**. Note that even if one includes Ising or Heisenberg coupling of a partially occupied f^{13} state, the lack of temperature dependence in the Yb XANES (**Figure 2**) is inconsistent with the valence tautomers postulate.

Returning to the experimental and theoretical work presented above, the available results overwhelmingly favor a mixed-configuration ground state giving rise to an otherwise conventional open-shell singlet with both intra- and intermolecular magnetic coupling, in which the former dominates the latter. This interpretation is supported by the Yb L_{III} XANES and magnetic susceptibility data, as well as the CASSCF calculations. The data and calculations place these compounds in the same class as cerocene as examples of intermediate valence in organometallic molecules where strong theoretical and experimental evidence exists supporting that view, and by implication also supports this view for the $\mathrm{Pn^*_2Ce}$,[22] $\mathrm{Ce[C_8H_4(Si^iPr_3\text{-}1,4)_2]_2}$,[23] and $[\mathrm{Ce}(\eta\text{-}\mathrm{C_5H_5})_3]^+$[24] systems.

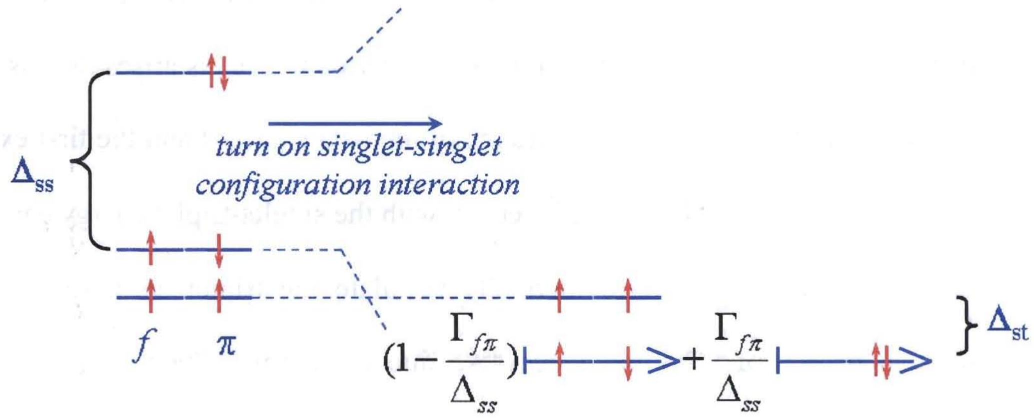

Figure 8. Cartoon energy-level diagram demonstrating the effect of a singlet-singlet configuration interaction on a singly-occupied f-orbital coupled with one unpaired electron in a ligand π orbital. In particular, the relative f^1 and f^0 component distributions are only schematic.

The qualitative picture that has now emerged is based on the seminal work of Neumann and Fulde[16] and further elaborated by Dolg, Fulde, Pitzer and co-workers[17, 18, 58] on the properties of cerocene. A qualitative energy-level diagram (**Figure 8**) demonstrates how the configuration interaction between the singlet states generates the multiconfigurational, intermediate valence, open-shell singlet ground state, simplifying the interactions to between one f electron and one electron on the ligand. As illustrated on the left side is the energy level diagram expected from Hund's rules with no overlap between the two metal and ligand orbitals, resulting in a triplet ground state. However, when one includes the configuration interaction between the singlet states, the splitting between these states (Δ_{ss}) increases, roughly inversely as the energy separation between the states. In a similar fashion, these states mix, generating the intermediate valence in the open-shell singlet configuration. The degree of mixing depends implicitly on the energy difference and the overlap between the two orbitals of the individual fragments used in constructing the open shell singlet, and such terms are lumped into the $\Gamma_{f\pi}$ coefficients in the qualitative model. If the splitting is large enough, the energy level of the open-shell singlet falls below that of the triplet. It should be noted that the open-shell singlet can be below the triplet only when the overlap is non-zero; however, the overlap must be small, and this situation is therefore rarely observed. If the overlap is large, a conventional closed-shell system represented by a single configuration with the two electrons delocalized between the two individual orbitals arises. In this case, the magnetism is set by a van Vleck mechanism that mixes the ground-state singlet and the first excited state triplet in the presence of a magnetic field, varying inversely with the singlet-triplet energy gap (Δ_{st}). When the temperature is high enough to start to thermally populate the triplet configuration, the susceptibility will initially increase, followed by a decrease due to thermal fluctuations, as in a conventional Curie-Weiss paramagnet. Within this qualitative picture (directly supported by the CASSCF calculations), there should be systems where the energies of the triplet and open shell singlet are nearly degenerate, or when the energies are more widely separated, the energy of the singlet can either be below or above the triplet. In these systems, the ground state will be close to trivalent, and the singlet state will be thermally populated.

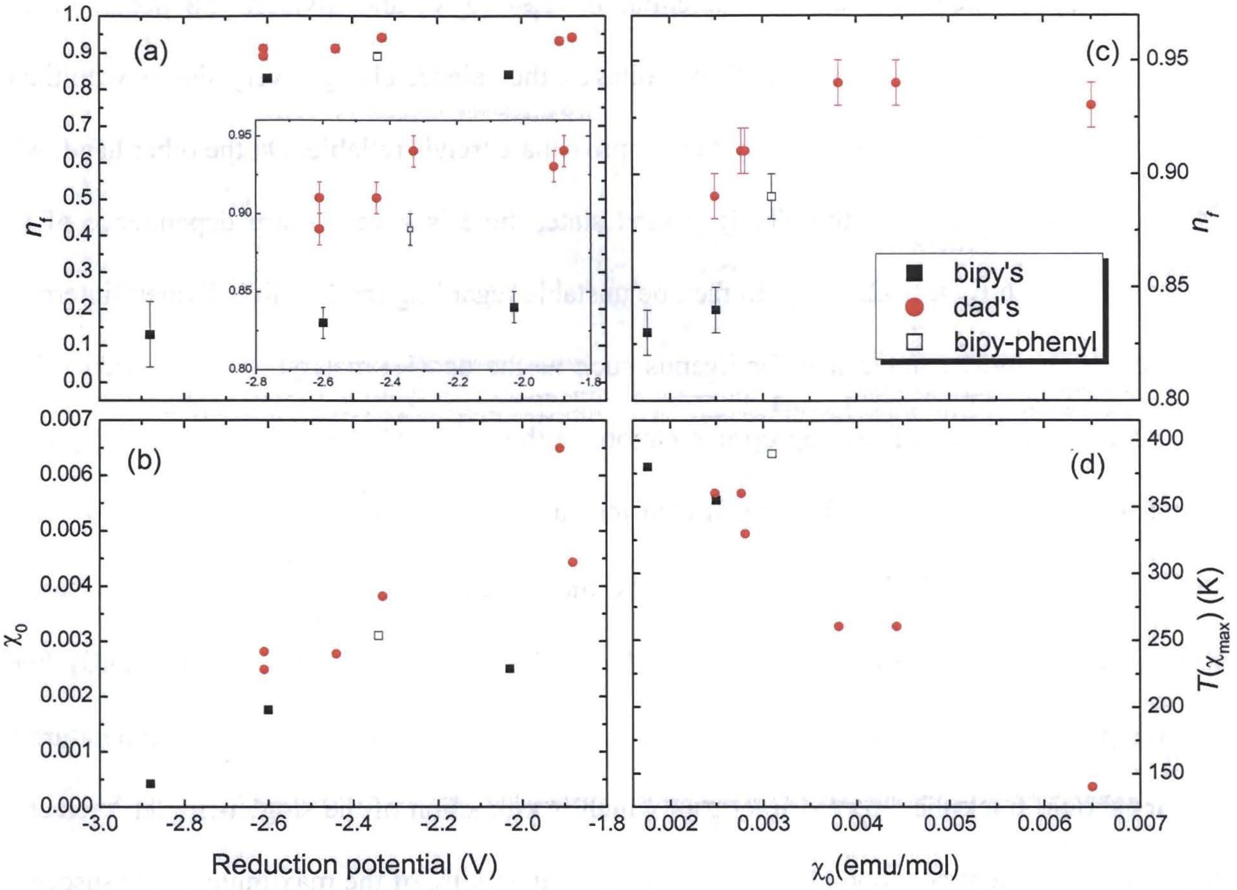

Figure 9. Plots of various correlated quantities from Table 1 for the Cp* coordination complexes. Errors on n_f are based on the fit covariance matrix and reproducibility. Absolute errors are about 5%.

The picture advocated above makes several qualitative predictions regarding the fundamental chemistry and physics that are consistent with the observed correlations between various parameters (**Figure 9**). First, although only a detailed theoretical treatments such as the CASSCF calculations described above are capable of making certain qualified predictions regarding the valence, more reducing ligands should generate stronger or pure divalent Yb character in this class of molecules as the magnitude of the reducing potential increases. This correlation is observed in the data summarized in Table 1, and is reflected in the CASSCF calculations by the degree of f/π* orbital overlap and the relative energy levels. The reduction potential data reported in Table 1 are a mix of values compiled from various sources, and hence errors of between 0.1 and 0.2 V are likely, but the range of potentials is wide enough that the relative values are useful for identifying general trends. In particular, close to trivalent Yb occurs when the reduction potential $E_r > \sim$-1.9 V, and divalent Yb occurs when this potential is near $E_r < \sim$-2.8 V. In between these voltages, the valence changes very slowly with the redox potential, making the identification of only such approximate trends reliable. On the other hand, when E_r is sufficiently negative to force the Yb(II) ground state, there is a very sharp dependence of the Yb valence. Ligands with E_r near -2.8 may, in fact, be unstable regarding the possible divalent/intermediate-valent states. It should be noted that for ligands such as the dad(H)-mesityl, the measured valence is indistinguishable from that of the appropriate cation, in this case, $[Cp^*_2Yb(dad(H)\text{-}p\text{-}tolyl]^+[BPh_4]^-$. In any event, the qualitative model (**Figure 8**) also indicates that as the degree of valence (or reduction potential) deviates from Yb(III) toward Yb(II), the magnitude of the TIP (χ_0) should decrease as an indicator of the singlet-singlet interaction, and within each series (dad- or bipy-based ligands) there is a strong correspondence. Likewise, the temperature at which the crossover to the high-temperature triplet state occurs should track the singlet-triplet gap, which is a function of the singlet-singlet interaction. In fact, there is an excellent correspondence between the temperature of the maximum in the susceptibility $T(\chi_{max})$ as a measure of the crossover temperature and χ_0 (**Figure 9d**).

One notable exception to these correlations occurs for Cp^*_2Yb(bipy(H)-phenyl). Despite its intermediate redox potential of -2.34 V, its valence and TIP behavior fall more in line with that of the dad ligands. This deviation is likely due to the limitation of using the reduction potential as the sole measure of f/π orbital overlap and mixing, as the π orbitals are potentially delocalized over a larger area in the bipy(H)-phenyl ligand than in the other bipy ligands studied here when the phenyl substituent is in partial conjugation with the bipy π^* system. In fact, the effect of the orientation of the 4,4'-diaryl substituents in the 4,4'-diaryl-2,2'-bipyridine derivatives and, therefore, the role delocalization plays in the photophysics of $[Ru(bipy)_3]^{2+}$ derivatives is understood.[59]

The implications of the multiconfigurational ground state contribution to the nature of the chemical bond is likely to be far reaching for the organometallic chemistry of certain lanthanide elements, yet have even broader implications that reach into device and metallic materials physics. This impact is due to the strong analogy to intermediate valence mechanisms in lanthanide intermetallics and related systems, as originally postulated by Neumann and Fulde[16] in their pioneering work, which draws the analogy between the singlet configuration interaction and the Kondo effect. The Kondo effect is relatively unfamiliar to chemists, but is largely responsible for a wide range of interesting electronic and magnetic behavior, from intermetallic intermediate valence,[2, 60] heavy-fermions[1, 60] and magnetically-mediated superconductivity,[61] to unusual transport behavior in single-molecule transistors,[62] and even quantum dots.[63] The effect is simply a coupling of a local magnetic moment to electrons in a conduction band and, ss such, is a complex many-body problem. Qualitatively, the coupling occurs when the magnetic orbitals hybridize with the conduction band, causing the formation of a quasibound singlet state, where some of the *f* electron weight is projected onto the conduction band and some of the electronic density in the conduction band is localized into the quasibound state, known as the "Kondo singlet." It was originally discovered in non-magnetic metals with a small magnetic impurity, where the electrical resistivity is observed to increase below a temperature where the Kondo coupling occurs.[64] As the temperature rises, the singlet breaks apart, and at temperatures well above the characteristic temperature scale T_K (essentially the singlet-triplet excitation energy), intermediate valence is destroyed, and a full moment Curie-Weiss paramagnetic state is recovered. However, at $T<T_K$, the slow breakup with increasing temperature of the singlet state (essentially governed by Boltzmann statistics) has a large effect on the magnetic moment, while maintaining a nearly temperature-independent, intermediate valent configuration on the metal.[65]

Using this analogy, the Kondo interaction in these organometallic molecules is the antiferromagnetic coupling between the magnetic moment on the metal and that on the ligand that effectively occurs due to the configuration interaction discussed above. The conduction band required by the Kondo model for the metal systems is then replaced by the aromatic, conjugated π orbitals, allowing for a strong hybridization with the otherwise local *f* states on the lanthanide, and thereby producing an intermediate valence state of the metal atom (that is, fractional *f* character).[65] In this environment, the antiferromagnetic coupling induces the formation of a quasi-bound singlet. The magnetic coupling therefore affects the spatial extent of the *f* and ligand orbitals. Continuing with this analogy, the results presented here have a particularly strong impact on understanding the magnetic properties of nanoparticles, surfaces, and devices, such as described in several recent studies.[66-72] In particular, these molecules form a clean system in which to study the Kondo effect on a molecular (i.e. nanoscale) level in a system free of the morphology difficulties of intermetallic nanoparticles.[73]

6. Conclusion

This article presents the Yb L_{III}-edge XANES, magnetism, and CASSCF calculational results on a number of bipyridine and diazabutadiene adducts to decamethylytterbocene. These results document an intermediate valence state for the ytterbium atom in each complex, forming a multiconfigurational open-shell singlet with the LUMO π^* ligand orbital. The degree of intermediate valence, or rather, closed-shell state mixing into the open-shell ground state, is found to be directly related to the antiferromagnetic coupling strength between the metal center and the ligand. These deductions, therefore, indicate that the origin of the unusual magnetic properties of these molecules is due to the intertwined nature of both a strong magnetic coupling strength and the electronic structure of the metal. The analogy of this molecular phenomenon to the Kondo effect in solid-state intermetallic magnetism continues to have predictive power, furthering the assertion that these organometallic molecules may be ideal systems with which to study the Kondo effect on the nanoscale. Finally, this study increases the number of molecules where this behavior is known to occur, and therefore has general implications for the nature of bonding in certain organolanthanide compounds.

The notion of multiconfigurational ground states is not common to chemists trained to think about molecules using a molecular orbital model. However, those trained to think in valence-bond language can readily understand the concept of multiconfigurational ground states. All students of chemistry know that the two resonance structures of benzene are described by individual wave functions, neither of which is the true wave function; the true wave function of benzene is composed of an admixture of these individual wave functions. The notion of multiconfigurational ground states in the ytterbocene complexes described in this article may be understood by a valence bond analogy. Thus, the individual wave functions for $Cp^*_2Yb(III,f^{13})(bipy^-)$ and $Cp^*_2Yb(II,f^{14})(bipy)$ are not the true wave function for the molecule $Cp^*_2Yb(bipy)$, but the true wave function is an admixture of the individual wave functions. Unlike benzene, however, the admixture is not 50:50, but changes depending on the ligands.

A physical picture that emerges is that although $Cp^*_2Yb(III,f^{13})(bipy^-)$ and $Cp^*_2Yb(II,f^{14})(bipy)$ differ with the former configuration being lower in energy than the latter, the electron in bipy in the Yb(III) configuration is in an antibonding π^* orbital. In addition the electron-electron repulsion in Yb(II) is greater than in Yb(III), with the net result that the valence bond structures are close in energy. Since the lanthanide molecules do not engage in covalence to any great extent, charge transfer from Yb(II) to the π^* orbital on bipy is not an available mechanism by which the molecule can relieve the electron-electron repulsion in the 4*f* shell. Rather, the molecule mixes the two ytterbium configurations into an intermediate valence configuration and therefore lowers the total energy of the molecule. In this sense, multiconfigurational ground states mimic covalence in systems where the valence electrons are core electrons, i.e. in certain lanthanide molecules.

Acknowledgments

This work was supported by the Director, Office of Science, Office of Basic Energy Sciences (OBES), of the U.S. Department of Energy (DOE) under Contract No. DE-AC02-05CH11231, and by the German Academic Exchange Service (DAAD) for a fellowship (MDW). X-ray absorption data were collected at the Stanford Synchrotron Radiation Laboratory, a national user facility operated by Stanford University on behalf of the DOE/OBES. Work at Los Alamos was performed under the auspices of the DOE. L.M thanks the CINES and CALMIP for a generous grant of computing time. L.M. is also member of the Institut Universitaire de France. L.M. and O.E thank the CNRS and Ministère de l'Enseignement Supérieur et de la Recherche for funding. We thank Martin Head-Gordon for enlightening discussions, Dr. Fred Hollander (at CHEXRAY, the U.C. Berkeley X-ray diffraction facility) for assistance with the crystallography, and Dr. Evan Werkema for his assistance.

Supporting Information Available

Full list of authors for reference 34. Magnetic susceptibility of several independent samples of $Cp^*_2Yb(bipy)$. Coordinates, in atomic unit, and level of calculations for each calculated species. Crystallographic data, labeling diagram, tables giving atomic positions, anisotropic thermal parameters, bond distances, bond angles, torsion angels, least square planes for $[Cp^*_2Yb(dad(H)\text{-}p\text{-}tolyl]^+[BPh_4]^-$. This material is available free of charge via the Internet at http://pubs.acs.org. Structure factor tables are available from the authors. Crystallographic data were also deposited with Cambridge Crystallographic Data Centre. Copies of the data (CCDC 699687) can be obtained free of charge via http://www.ccdc.cam.ac.uk/data_request/cif by e-mailing data_request@ccdc.cam.ac.uk, or by contacting The Cambridge Crystallographic Data Centre, 12, Union Road, Cambridge CB 1EZ, UK; fax +44 1223 336033.

REFERENCES

(1) Hewson, A. C., *The Kondo Problem to Heavy Fermions*. Cambridge University Press: Cambridge, 1993.

(2) Lawrence, J. M., Intermediate Valence Compounds. In *Encyclopedia of Physics*, 2nd ed.; Lerner, R. G.; Trigg, G. L., VCH Publishers: New York, 1991; Vol. pp.

(3) Stewart, G. R., *Rev. Mod. Phys.* **1984,** *56*, 755.

(4) Schultz, M.; Boncella, J. M.; Berg, D. J.; Tilley, T. D.; Andersen, R. A., *Organometallics* **2002,** *21*, 460.

(5) Walter, M. D.; Berg, D. J.; Andersen, R. A., *Organometallics* **2006,** *25*, 3228.

(6) Veauthier, J. M.; Schelter, E. J.; Kuehl, C. J.; Clark, A. E.; Scott, B. L.; Morris, D. E.; Martin, R. L.; Thompson, J. D.; Kiplinger, J. L.; John, K. D., *Inorg. Chem.* **2005,** *44*, 5911.

(7) Walter, M. D.; Berg, D. J.; Andersen, R. A., *Organometallics* **2007,** *26*, 2296.

(8) Veauthier, J. M.; Schelter, E. J.; Carlson, C. N.; Scott, B. L.; Da Re, R. E.; Thompson, J. D.; Kiplinger, J. L.; Morris, D. E.; John, K. D., *Inorg. Chem.* **2008,** *47*, 5841.

(9) Benelli, C.; Caneschi, A.; Gatteschi, D.; Sessoli, R., *Inorg. Chem.* **1993,** *32*, 4797.

(10) Benelli, C.; Caneschi, A.; Gatteschi, D.; Sessoli, R., *J. Appl. Phys.* **1993,** *73*, 5333.

(11) Benelli, C.; Gatteschi, D., *Chem. Rev.* **2002,** *102*, 2369.

(12) Caneschi, A.; Dei, A.; Gatteschi, D.; Massa, C. A.; Pardi, L. A.; Poussereau, S.; Sorace, L., *Chem. Phys. Lett.* **2003,** *371*, 694.

(13) Caneschi, A.; Dei, A.; Gatteschi, D.; Poussereau, S.; Sorace, L., *Dalton Trans.* **2004**, 1048.

(14) Sanada, T.; Suzuki, T.; Yoshida, T.; Kaizaki, S., *Inorg. Chem.* **1998,** *37*, 4712.

(15) Tsukuda, T.; Suzuki, T.; Kaizaki, S., *J. Chem.. Soc., Dalton Trans.* **2002**, 1721.

(16) Neumann, C.-S.; Fulde, P., *Z. Phys. B* **1989,** *74*, 277.

(17) Dolg, M.; Fulde, P.; Küchle, W.; Neumann, C.-S.; Stoll, H., *J. Chem. Phys.* **1991,** *94*, 3011.

(18) Dolg, M.; Fulde, P.; Stoll, H.; Preuss, H.; Chang, A.; Pitzer, R. M., *Chem. Phys.* **1995,** *195*, 71.

(19) Booth, C. H.; Walter, M. D.; Daniel, M.; Lukens, W. W.; Andersen, R. A., *Phys. Rev. Lett.* **2005,** *95*, 267202.

(20) Edelstein, N. M.; Allen, P. G.; Bucher, J. J.; Shuh, D. K.; Sofield, C. D.; Kaltsoyannis, N.; Maunder, G. H.; Russo, M. R.; Sella, A., *J. Am. Chem. Soc.* **1996,** *118*, 13115.

(21) Amberger, H. D.; Reddmann, H.; Edelmann, F. T., *J. Organomet. Chem.* **2005,** *690*, 2238.

(22) Ashley, A.; Balazs, G.; Cowley, A.; Green, J.; Booth, C. H.; O'Hare, D., *Chem. Comm.* **2007**, 1515.

(23) Balazs, G.; Cloke, F. G. N.; Green, J. C.; Harker, R. M.; Harrison, A.; Hitchcock, P. B.; Jardine, C. N.; Walton, R., *Organometallics* **2007,** *26*, 3111.

(24) Coreno, M.; de Simone, M.; Green, J. C.; Kaltsoyannis, N.; Narband, N.; Sella, A., *Chem. Phys. Lett.* **2006,** *432*, 17.

(25) Walter, M. D.; Schultz, M.; Andersen, R. A., *New J. Chem.* **2006,** *30*, 238.

(26) Keski-Rahkonen, O.; Krause, M. O., *Atomic Data and Nuclear Data Tables* **1974,** *14*, 139.

(27) Sarrao, J. L.; Immer, C. D.; Fisk, Z.; Booth, C. H.; Figueroa, E.; Lawrence, J. M.; Modler, R.; Cornelius, A. L.; Hundley, M. F.; Kwei, G. H.; Thompson, J. D.; Bridges, F., *Phys. Rev. B* **1999,** *59*, 6855.

(28) Teo, B. K., *EXAFS : basic principles and data analysis* Springer-Verlag: New York, 1986.

(29) O'Connor, C. J., In *Progress in Inorganic Chemistry*, ed.; Lippard, S. J., J. Wiley & Sons: 1982; Vol. 29, pp. 203.

(30) Dolg, M.; Stoll, H.; Preuss, H., *J. Chem. Phys.* **1989,** *90*, 1730.

(31) Dolg, M.; Stoll, H.; Savin, A.; Preuss, H., *Theor. Chim. Acta* **1989,** *75*, 173.

(32) Dolg, M.; Stoll, H.; Preuss, H., *Theor. Chim. Acta* **1993,** *85*, 441.

(33) Hariharan, P. C.; Pople, J. A., *Theor. Chim. Acta* **1973,** *28*, 213.

(34) Frisch, M. J. *et al.*, *Gaussian 98, Revision A-11*. Gaussian, Inc.: Pittsburgh PA, 2001.

(35) Becke, A. D., *J. Chem. Phys.* **1993,** *98*, 5648.

(36) Burke, K.; Perdew, J. P.; Yang, W. In *Electronic Density Functional Theory: Recent Progress and New Directions*, 1998; Dobson, J. F.; Vignale, G.; Das, M. P., Ed. Plenum: New York: 1998.

(37) Casida, M. E.; Jamorski, C.; Casida, K. C.; Salahub, D. R., *J. Chem. Phys.* **1998,** *108*, 4439.

(38) Moore, J. A. Ph. D. Thesis; University of Texas, Austin, 2006.

(39) Coulombeix, J.; Emmenegger, F. P., *Helv. Chim. Acta* **1985,** *68*, 248.

(40) Dieck, H. T.; Renk, I. W., *Chem. Ber.* **1971,** *104*, 110.

(41) Tilley, T. D.; Andersen, R. A.; Spencer, B.; Zalkin, A., *Inorg. Chem.* **1982,** *21*, 2647.

(42) Griffith, J. S., On the general theory of magnetic susceptibilities of polynuclear transition-metal compounds. In *Structure and Bonding*, ed.; Spinger-Verlag: New York, 1972; Vol. 10, pp. 87.

(43) Fisher, M. E., *Am. J. Phys.* **1964,** *32*, 343.

(44) Bonner, J. C.; Fisher, M. E., *Phys. Rev.* **1964,** *135*, A640.

(45) Estes, W. E.; Gavel, D. P.; Hatfield, W. E.; Hodgson, D. J., *Inorg. Chem.* **1978,** *17*, 1415.

(46) Lines, M. E., *J. Chem. Phys.* **1971,** *55*, 2977.

(47) Lueken, H.; Hannibal, P.; Handrick, K., *Chem. Phys.* **1990,** *143*, 151.

(48) The singlet CASSCF calculation has been carried out by calculating two roots that correspond to the open-shell and the closed-shell singlet. However, the closed-shell system has also been

optimized separately at the CASSCF level, confirming that this state is higher in energy than the corresponding open-shell singlet.

(49) Trifonov, A. A.; Kirillov, E. N.; Bochkarev, M. N.; Schumann, H.; Muehle, S., *Russ. Chem. Bull.* **1999,** *48*, 381.

(50) Trifonov, A. A.; Kurskii, Y. A.; Bochkarev, M. N.; Muehle, S.; Dechert, S.; Schumann, H., *Russ. Chem. Bull.* **2003,** *52*, 601.

(51) Lea, K. R.; Leask, M. J. M.; Wolf, W. P., *J. Phys. Chem. Solids* **1962,** *23*, 1381.

(52) Gerloch, M.; Constable, E. C., *Transition Metal Chemistry*. VCH: Weinheim, 1995.

(53) Pierpont, C., *Coord. Chem. Rev.* **2001,** *216-217*, 99.

(54) Roux, C.; Adams, D. M.; Itie, J. P.; Polian, A.; Hendrickson, D. N.; Verdaguer, M., *Inorg. Chem.* **1996,** *35*, 2846.

(55) LaBute, M. X.; Kulkarni, R. V.; Endres, R. G.; Cox, D. L., *J. Chem. Phys.* **2002,** *116*, 3681.

(56) Da Re, R. E.; Kuehl, C. J.; Brown, M. G.; Rocha, R. C.; Bauer, E. D.; John, K. D.; Morris, D. E.; Shreve, A. P.; Sarrao, J. L., *Inorg. Chem.* **2003,** *42*, 5551.

(57) Carlson, C. N.; Kuehl, C. J.; Ogallo, L.; Shultz, D. A.; Thompson, J. D.; Kirk, M. L.; Martin, R. L.; John, K. D.; Morris, D. E., *Organometallics* **2007,** *26*, 4234.

(58) Dolg, M.; Fulde, P., *Chem. Eur. J.* **1998,** *4*, 200.

(59) Damraner, N. H.; Boussie, T. B.; Devenney, M.; McCusker, J. K., *J. Am. Chem. Soc.* **1997,** *119*, 8253.

(60) Fulde, P.; Keller, J.; Zwicknagl, G., *Solid State Physics* **1988,** *41*, 1.

(61) Mathur, N. D.; Grosche, F. M.; Julian, S. R.; Walker, I. R.; Freye, D. M.; Haselwimmer, R. K. W.; Lonzarich, G. G., *Nature* **1998,** *394*, 39.

(62) Liang, W.; Shores, M. P.; Bockrath, M.; Long, J. R.; Park, H., *Nature* **2002,** *417*, 725.

(63) Goldhaber-Gordon, D.; Shtrikman, H.; Mahalu, D.; Abusch-Magder, D.; Meirav, U.; Kastner, M. A., *Nature* **1998,** *391*, 156.

(64) De Haas, W. J.; De Boer, J.; Van Den Berg, G. J., *Physica* **1934,** *1*, 1115.

(65) Bickers, N. E.; Cox, D. L.; Wilkins, J. W., *Phys. Rev. B* **1987,** *36*, 2036.

(66) Thimm, W. B.; Kroha, J.; von Delft, J., *Phys. Rev. Lett.* **1999,** *82*, 2143.

(67) Schlottmann, P., *Phys. Rev. B* **2001,** *65*, 024420.

(68) Schlottmann, P., *Phys. Rev. B* **2001,** *65*, 022431.

(69) Schlottmann, P., *Phys. Rev. B* **2002,** *65*, 174407.

(70) Huang, P.; Carter, E. A., *Nano Lett.* **2006,** *6*, 1146.

(71) Zhao, A.; Li, Q.; Chen, L.; Xiang, H.; Wang, W.; Pan, S.; Wang, B.; Xiao, X.; Yang, J.; Hou, J. G.; Zhu, Q., *Science* **2005,** *309*, 1542.

(72) Osorio, E. A.; O'Neill, K.; Wegewijs, M.; Stuhr-Hansen, N.; Paaske, J.; Bjornholm, T.; van der Zant, H. S. J., *Nano Lett.* **2007,** *7*, 3336.

(73) Han, S.-W.; Booth, C. H.; Bauer, E. D.; Huang, P. H.; Lawrence, J. M.; Chen, Y. Y., *Phys. Rev. Lett.* **2006,** *97*, 097204.

SYNOPSIS TOC

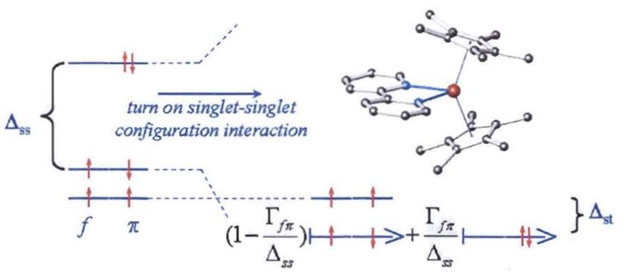

Los Alamos
NATIONAL LABORATORY
EST.1943

Technical Information Release

IRM-RMMSO
reviewandapproval@lanl.gov

Reserved for Classification Group (SAFE-1)

LA-UR

LA-CP

Submit to Classification Group (SAFE-1), MS F674, TA-3-1400, Rm 3475, the following, in order and clipped (not stapled) together:
- ✓ This form, blocks 1-8 completed
- ✓ Appropriate cover sheet (Form 836 for LA-UR, Form 1756a-e for LA-CP)
- ✓ **1 copy** (double-sided for paper, if practical) of STI product

For world-wide web content, provide signed form and secure url address to web_standards@lanl.gov.

1. Author(s) (*Include all contributing authors; first must be LANL employee.*)

Last	First	Middle	Z No.	Group or affiliation
Booth	C	H		LBNL
Walter	M	C		LBNL
Kazhdan	D			LBNL

(see attached for full author list)

2. Primary Responsible Author: *My signature attests to the integrity and validity of the information provided on this form and the associated STI product, and affirms that all authors concur with its publication.*

Printed Name: Eric Bauer
Signature:
Date:

3. Document Title (use upper/lower case; spell out symbols)

Decamethylytterbocene Complexes of Bipyridines and Diazabutadienes: Multiconfigurational Ground States and Open-shell Singlet Formation

4. Type of Information

☐ Abstract ☒ Full Paper/Report
☐ Summary ☐ Poster
☐ Audio-Visual (*abstract required*)
☐ Viewgraphs/Presentations (*abstract required*)
☐ Other: ______

Intended for:
☒ Journal ☐ Proceedings ☐ Meeting ☐ Talk ☐ Book ☐ World-wide Web
☐ Book Chapter ☐ Electronic (e.g. e-print archive) ☐ Other: ______

Particulars: (**see point # 4 of instruction sheet.**)
Meeting/Conf. Name: ______
City, State, and Country: ______ Mtg. Date: ______
Journal Name: Journal of the American Chemical Society
Other: ______

5. Research sponsored by
☒ DOE/LANL/LDRD ☐ DHS ☐ DOD ☐ Other: ______

Program Code used for this work: E415

6. Deadline Date

Z Number, name, e-mail, and phone number of contact for notification of release
079449, Juanita Armijo, juanitaa@lanl.gov, 7-4838

7. Classification Category (***Cite applicable DUSA or obtain Derivative Classifier review***)
☒ Unclassified
Applicable DUSA Designator:

☒ Unclassified ☐ Classified ☐ Unclassified, controlled; Category: ______
Derivative Classifier Name: Michael Hundley
Signature:
Date:

8. Responsible Line Manager: *Consistent with my responsibilities and authorities, my signature certifies that I have reviewed this STI product for professional, contractual, programmatic, institutional, and patent sensitivities, and that I concur with its publication.*

Printed Name:
Signature:
Date:

To be completed by Classification Group, SAFE-1

Date Received	OSTI Category	Date Released
Classification Analyst Signature	☐ U ☐ C ☐ S ☐ RD ☐ FRD ☐ NSI ☐ UCNI ☐ OUO	

Comments:

To be completed by IRM-RMMSO

OSTI Distribution ☐ Yes ☐ No
Record Copy to Research Library ☐ Yes ☐ No

Form 678 (7/08)